RNA-seq-based genome reannotation of dermatophyte *Arthroderma benhamiae*, characterization of its secretome and whole gene expression profile during infection

Van Du T. Tran[1ǂ], Niccolò De Coi[2ǂ], Marc Feuermann[3], Emanuel Schmid-Siegert[1], Elena-Tatiana Băguţ[4], Bernard Mignon[4], Patrice Waridel[5], Corinne Peter[6], Sylvain Pradervand[6], Marco Pagni[1*#], Michel Monod[2*#]

[1] Vital-IT group, SIB Swiss Institute of Bioinformatics, Lausanne, Switzerland

[2] Department of Dermatology, Centre Hospitalier Universitaire Vaudois, Lausanne, Switzerland

[3] Swiss-Prot group, SIB Swiss Institute of Bioinformatics, Geneva, Switzerland

[4] Fundamental and Applied Research for Animals & Health (FARAH), Department of Infectious and Parasitic Diseases, Faculty of Veterinary Medicine, University of Liège, Liège, Belgium

[5] Protein Analysis Facility, Center for Integrative Genomics, University of Lausanne, Lausanne, Switzerland

[6] Genomic Technologies Facility, Center for Integrative Genomics, University of Lausanne, Lausanne, Switzerland

Running title: *A. benhamiae* genome reannotation and gene expression

Key words: *Arthroderma benhamiae*, *Trichophyton*, dermatophytes, RNA-seq, annotation, infection, secreted proteins, proteases

♮ These authors contributed equally to this work

* Joint senior authors of this work

Corresponding authors

Dr. Marco Pagni, Vital-IT group, SIB Swiss Institute of Bioinformatics, Quartier Sorge, bâtiment Génopode, 1015 Lausanne, Switzerland. Email: Marco.Pagni@isb-sib.ch. Tel: +41 21 692 40 38. Fax: +41 21 692 40 65.

Professor Michel Monod, Department of Dermatology, Centre Hospitalier Universitaire Vaudois, BT422, 1011 Lausanne, Switzerland. E-mail**:** Michel.Monod@chuv.ch. Tel: + 41 21 314 03 76. Fax: + 41 21 314 03 78.

ABSTRACT

Dermatophytes are the most common agents of superficial mycoses in humans and animals. The aim of the present investigation was to systematically identify the extracellular, possibly secreted, proteins that are putative virulence factors and antigenic molecules of dermatophytes. A complete gene expression profile of *Arthroderma benhamiae* was obtained during infection of its natural host (guinea pig) using RNA-seq technology. This profile was completed with those of the fungus cultivated *in vitro* in two media containing keratin and soy meal protein as the sole source of nitrogen, and in Sabouraud medium. More than 60% of transcripts deduced from RNA-seq data differ from those previously deposited for *A. benhamiae*. Using these RNA-seq data along with an automatic gene annotation procedure, followed by manual curation, we produced a new annotation of the *A. benhamiae* genome. This annotation comprised 7405 CDSs, among which only 2662 were identical to the currently available annotation, 383 were newly identified, and 15 secreted proteins were manually corrected. The expression profile of genes encoding proteins with a signal peptide in infected guinea pigs was found very different from that during *in vitro* growth when using keratin as substrate. Especially, the sets of the 12 most highly expressed genes encoding proteases with a signal sequence only had the putative vacuolar aspartic protease gene *PEP2* in common, during infection and in keratin medium. The most upregulated gene encoding a secreted protease during infection was that encoding subtilisin SUB6, which is a known major allergen in the related dermatophyte *Trichophyton rubrum*.

IMPORTANCE

Dermatophytoses (ringworm, jock itch, athlete's foot and nail infections) are the most common fungal infections, but their virulence mechanisms are poorly understood. Combining transcriptomic data obtained from growth in various culture conditions with data obtained during infection led to a significantly improved genome annotation. About 65% of the protein-coding genes predicted with our protocol did not match the existing annotation for *A. benhamiae*. Comparing gene expression during infection on guinea pigs versus keratin degradation *in vitro*, which is supposed to mimic the host environment, revealed the critical importance of using real *in vivo* conditions for investigating virulence mechanisms. The analysis of genes expressed *in vivo*, encoding cell surface and secreted proteins, particularly proteases, led to the identification of new allergen and virulence factor candidates.

INTRODUCTION

Pathogenic dermatophytes are the most common agents of superficial mycoses, almost exclusively infecting the *stratum corneum*, nails, and hair (1, 2). The genomes of these fungi, smaller in size than those of *Aspergillus* spp., range from 22.5 to 24 Mb and are highly collinear. The number of predicted protein-coding genes varies from 7980 in *Arthroderma benhamiae* to 8915 in *Microsporum canis*. (3, 4). A large number of orthologs were found to be shared by all dermatophytes (6158 groups including paralog duplications) (4). Dermatophyte genomes were found to be enriched in genes encoding secreted proteases and depleted in genes encoding enzymes involved in sugar metabolism, as for example those typically involved in plant cell wall breakdown. These differences with other fungi attest to the high specialization of dermatophytes and their adaptation to particular proteinaceous substrates other than vegetal debris.

The molecular mechanisms involved in the establishment of dermatophyte infections are poorly understood and remain an open field of investigation. Host–fungus interactions involve pathogen offence, host defense and pathogen counter-attack. In these processes, fungal and host cell-associated and secreted proteins play a major role. For instance, secreted aspartic proteases are now considered important virulence factors of *Candida albicans*, being associated with adhesion, invasion, and tissue damage (5). Secreted enzymes referred to as ‘effectors’ are also of major importance for host attack by plant pathogens (6). Likewise, proteins secreted *in vivo*, in particular proteases, are clearly the best candidates for virulence factors of dermatophytes.

Current knowledge regarding dermatophyte gene expression during infection was acquired using a cDNA microarray based on transcripts of *A. benhamiae*, grown in a

protein medium, covering approximately 20–25% of its genome and on few selected protease-coding genes (7). As a striking result, the genes encoding most major proteases secreted by the fungus *in vitro* (8–11) were found to be not expressed *in vivo* and, therefore, these proteases appeared not to be involved during the establishment of infection. In contrast, the gene encoding the subtilisin SUB6 was found to be highly expressed during skin infection, but not when the fungus grew in any culture medium. Of particular importance, SUB6 is the ortholog of the major allergen Tri r2 in *T. rubrum* (12). Tri r2 was found to induce dual immune responses and elicit either immediate or delayed-type hypersensitivity skin test reactions in different individuals. Numerous antigenic molecules eliciting host immune responses still remain to be discovered. In view of the importance of secreted proteins, both as antigens and as possible virulence factors, the goals of this work were the following: (i) to obtain a complete gene expression profile of *A. benhamiae* during infection using state-of-the-art RNA-seq technology, (ii) to compare it with the expression profiles of the fungus grown *in vitro* in different media and (iii) to identify which proteins, and in particular individual proteases, are secreted *in vivo* during infection as possible new virulence factors. By exploiting RNA-seq data of *A. benhamiae* growing in different culture conditions and during infection in guinea pigs, we first established a new annotation of the genome, with 7405 protein-coding genes. The previously available genome annotation of *A. benhamiae* showed its limits, as many discrepancies were found after comparison with new experimental data.

RESULTS

Arthroderma benhamiae experimental infections in guinea pigs

Skin samples from experimentally infected animals were used for transcriptomic analysis of *A. benhamiae* during infection. As shown in Fig. 1, at day 8 after infection, the animals showed no or minimal skin symptoms. The direct mycological examination showed numerous filaments present on the hair and skin samples with the presence of a low number of conidia (data not shown). At 14 days, the guinea pigs exhibited macroscopic skin lesions, but direct mycological examination showed fewer fungal filaments on the infected skin samples with thicker septa than at 8 days. We considered day 8 as the time point for the peak of infection and day 14 as the time point for the peak of inflammation. After 27 days, the skin lesions were still present but regressing, while very few fungal elements were observed by direct mycological examination. At day 44, the guinea pigs had fully recovered from infection, and no *A. benhamiae* filaments were observable. At this time, three animals that had recovered from primary infection were reinfected by *A. benhamiae* but did not develop a new infection.

RNA sequencing

RNA was extracted in triplicate from the fungus grown in keratin medium, soy protein medium, and Sabouraud medium and from each infected animal. Approximately 13 million strand-specific reads were obtained for each RNA sample extracted from the fungus growing in the three tested culture media (Table 1). Approximately 30 million strand-specific reads were acquired from each RNA sample extracted from infected skin samples, consisting of a mixture of reads from the fungus and from its mammalian host. As a result,

roughly 1 million fungal reads (2.8%) were obtained with RNA extracted from skin samples of guinea pigs at day 8 of infection, while 91.3% of the reads could be aligned with the guinea pig genome.

New gene annotation of the *Arthroderma benhamiae genome*

A preliminary investigation of the RNA-seq reads mapped onto the *A. benhamiae* genome revealed that many gene and intron locations from the original genome annotations were not supported by our experimental data. Hence, re-annotating the CDS of the genome appeared to be a prerequisite before further analyzing the transcriptome expression. Particular attention was paid to the location of the start codons because of our interest in secreted proteins, which should be endowed with a signal peptide at the N-terminus.

We used *augustus* (13), a program for gene prediction in eukaryotic organisms that relies on a statistical model of an organism's gene structure. The correctness of *augustus* predictions is, however, highly dependent on this model, and great care must be used at the time of training this model (i.e., establishing the model using a training dataset). Practically, we mapped all RNA-seq reads onto the genome, deduced full-length gene transcripts, and retained only those with sufficient coverage. Then, we translated the filtered transcripts into their three possible coding frames. Full-length CDS were detected by aligning the transcripts against a set of high-quality protein sequences, namely the protein sequences reviewed by Swiss-Prot of the model organisms *S. cerevisiae* and *A. nidulans*. The CDS annotations were back-propagated onto the genome, introducing intron descriptions, and supplied as a training set to *augustus* to generate a new gene model. With the latter, the *A. benhamiae* genome was re-annotated and yielded 7405 protein-coding genes.

Table 2 compares our 7405 newly predicted genes with the original set of 7979 and shows that about 65% of the genes have been affected one way or another, for example the intron boundaries within 1246 genes were corrected and 383 new genes were recorded. In addition, 39 genes in the existing annotation were split into two genes, and, in contrast, 286 genes in the new annotation corresponded to fusions of previously annotated genes.

In silico definition of the secretome

We defined the *secretome* as the set of all secreted proteins, which is made of all proteins with a signal peptide, excluding trans-membrane proteins. In practice, this set is not trivial to define. The presence/absence of a signal peptide depends on the tools used to predict it, on the strength of the signal itself, and on its presence at the N-terminus, which ultimately relies on the correct detection of the start codon. Hence, all genes predicted by *augustus* were further subjected to prediction refinements as follows. For every predicted CDS, variants were enumerated by considering every AUG or CUG (14) as an alternative start codon, when found within 30 amino acids from the AUG given by *augustus*. Signal peptides were then searched for in all CDS variants. The retained CDS was finally selected manually by comparing the results of the different predictions and by considering additional evidence, such as prior biological knowledge or the presence of a GPI anchor at the C-terminus. GPI anchors affect the localization of these proteins in the plasma membrane or the cell wall, but removal of the GPI lipid moiety by phospholipases can generate soluble secreted forms of the protein (15). The overall procedure of gene prediction followed by manual correction is summarized with an example in Fig. 2.

A total of 634 proteins with a signal peptide, including 112 probable GPI-anchored proteins, have been predicted. Using transmembrane predictors, we removed all proteins that contained one or more transmembrane spans in addition to the signal peptide and that were probably targeted to membranes. This refinement led to a final *A. benhamiae* predicted secretome, made of 457 proteins that are listed and characterized in Table S1.

A handful of *A. benhamiae* proteins have been experimentally characterized, in particular secreted proteases (16) and hydrophobin HypA (17). In order to associate functional information to predicted proteins, we searched for homologs using Blast against UniProtKB (18), paying particular attention to the matches against *S. cerevisiae*, the best characterized fungus; *C. albicans*, the best characterized yeast pathogen; and filamentous fungi, such as *Aspergillus* spp. We completed functional predictions by checking for the presence of specific domains or protein family signatures by scanning the InterPro database (19, 20). We were able to associate putative functions to 316 out of our 457 predicted cell surface/secreted proteins, including main functional groups such as proteases, carbohydrate/cell wall metabolism proteins or proteins with lipolytic activities (see Fig. 3A and Supplementary Results for details). In addition to thaumatin-like proteins, we identified 46 gene products showing homologies to known allergens (Table S2), of which 21 were predicted to be secreted. Among the 141 uncharacterized secreted proteins, 25 had homologs in other dermatophytes, suggesting they are involved in dermatophyte-specific functions/processes.

Validation of the new gene predictions of the secretome

The secretome can be relatively easily subjected to investigation by MS because it represents a small fraction of all proteins, and those found in the supernatant of *in vitro*

grown cultures can be recovered easily. We conducted a new analysis of the MS data we previously published (16) regarding proteins secreted by cells grown in soy protein liquid medium, using the new secretome definition. The presence of 139 proteins in the supernatant at either pH 4 or 7 was confirmed (Table S1), including 8 of the newly predicted ones. Moreover, among the 708 proteins from the original annotation that were lost in our new prediction, 31 were supposed to be secreted, but none of them could be detected in our MS data.

Similarity search is another way to test the quality of gene prediction. As an example, ARB_07403 encodes a putative A1 peptidase. In our prediction, ARB_07403 was shortened at the N-terminus by 68 residues. This correction not only allows for the identification of a strong signal peptide at the new N-terminus but also aligns better with the sequences of orthologs in closely related species, including TRV_06366 of *Trichophyton verrucosum* (UniProt D4DGR1) and MCYG_07979 of *Arthroderma otae* (UniProt C5FZ57).

However, it happens that neither prediction fitted with related proteins, requiring a further step of manual sequence correction. ARB_06467 (SUB10) and ARB_04678 (SED3) were found by similarity search to belong to respectively the S8 and S53 families of serine proteases, but the predicted proteins missed the N-terminal signal peptide and pro-peptide. A reanalysis of the nucleotide sequence of SUB10 revealed a probable genome assembly error in a poly-T stretch localized just behind the actual initiator codon, leading to a frameshift at position 4 (Fig. S1A). An error was also identified within the coding sequence of ARB_04677, upstream of ARB_04678. Correcting this error removed a frameshift at residue 109 of ARB_04677 and led to the fusion of the two ORFs (Fig. S1B). Sanger re-sequencing of the regions surrounding the two predicted errors confirmed our predictions

and allowed us to restore both protease sequences with clear signals and pro-peptides. The actual protein sequences of SUB10 and SED3 have been updated in the UniProtKB database (D4AQG0 and D4AK75 respectively).

Finally, it is interesting to note that, within the 40 new predicted ORFs, sequence alignments with other fungal proteomes revealed that two have homologs in filamentous fungi, such as *Aspergilli* species, and 22 are conserved in other dermatophyte species (Table S1).

Arthroderma benhamiae **gene expression in different growth conditions**

Gene expression levels were computed by mapping the reads onto the newly predicted gene set and are expressed as TMM-normalized Voom-transformed counts (Table S3). The nomenclature used for the samples and the corresponding growth conditions are given in Table 3. Fig. 4 presents an overview of the gene expression in the different samples, considering either the complete genome or the secretome subset. Both hierarchical clustering and principal component analysis indicate that the biological replicates are closer to each other than to other conditions, even for the *in vivo* samples at 14 days post infection, where the number of obtained fungal reads (about 50000) is possibly too low to perform a statistically significant analysis. However, the small distinction between the Gp8 and Gp14 *in vivo* conditions which is on the order of intra-Gp variations seems to indicate the consistency of Gp14 samples.

The expression differences are strongly dominated by the contrast between *in vivo* Gp8+Gp14 and *in vitro* S+Sa+K conditions. This result confirms and generalizes the observations made previously on a much smaller gene set (7). The analysis of the

expression data from the complete genome (including the secretome) and of the secretome yielded the same strong contrast, possibly even slightly reinforced for the secretome.

Among the *in vitro* conditions, the gene expressions in the soy and Sabouraud media appeared closer to each other in the complete gene set, while soy and keratin appeared closer in the secretome subset. None of the three *in vitro* conditions tested is a good proxy for *in vivo* growth conditions, despite the keratin medium being supposed to mimic the host environment. To address this question in more depth, we enumerated all possible partitions of growth conditions into two subsets, to contrast a subset of conditions versus the remaining ones. The list of all possible contrasts is given in Fig. 5, with the corresponding amounts of differentially expressed genes. This confirms that the *in vivo* versus *in vitro* contrast is dominant and that not much information can be expected to be gathered by separating Gp8 from Gp14. Interestingly, two other contrasts seem to carry additional signals: K:Gp8+Gp14+Sa+S in the genome complete gene set and Gp8+Gp14+Sa:S+K in the secretome subset.

We utilized a different statistical approach, namely WGCNA and gene ontology enrichment analysis, to further explore these additional contrasts. The unsupervised clustering algorithm of WGCNA subdivided the input gene set (genome) into 35 different modules, which are disjoint subsets of genes. Then, these modules were individually correlated with the 15 possible different contrasts to detect optimal correlations. As shown in Fig. S2, the *in vivo* versus *in vitro* contrast is again dominating the results, with 2122 genes found in the *turquoise* and *blue* modules. Fig. S3A presents the gene expression heatmap for the *turquoise* module as an example. The *blue* module also showed a high correlation with the *in vivo* versus *in vitro* contrast, although the expression in Sabouraud

was intermediate (Fig. S3B). A few other smaller modules appeared to be correlated with different contrasts, such as the *tan* module with 209 genes that strongly correlates with K:Gp8+Gp14+Sa+S (Fig. S3C) and the *midnightblue* module with 177 genes, highly correlating with Gp8+Gp14+S:K+Sa (Fig. S3D). The 323 genes from the *yellow* module also correlate with Gp8+Gp14+S:K+Sa, despite an intermediate expression in Sabouraud (Fig. S3E).

We mapped about 40% of the predicted proteins of *A. benhamiae* to their orthologous counterpart in *S. cerevisiae* using *inparanoid* and propagated the latter GO annotations onto the dermatophyte genes. Table S4 presents the modules for which the most significant GO term enrichment was detected, especially the *yellow*, *midnightblue* (correlated with K+Sa:Gp8+Gp14+S) and *tan* (correlated with K:Gp8+Gp14+Sa+S) modules. The results are, however, very general, revealing changes in translational and RNA-related activities but also indicate that some proteasome-related activities might be specifically altered during growth on keratin. These somewhat modest results are certainly more related to the lack of specific gene annotation for *A. benhamiae* than to a lack of well-formed gene modules.

Gene expression profile of *Arthroderma benhamiae* cell surface/secreted proteins during inflammatory cutaneous infection highly differs from the profile obtained during growth on keratin

Fig. 6A lists the 25 secretome genes most highly expressed *in vivo*, including five putative protease genes. The first gene, ARB_01183, encodes a protein which contains a thaumatin domain. The second gene, ARB_05307, encodes the subtilisin SUB6. Four genes encode proteins for which we did not find any functional data. These include ARBNEW_231, a

303 newly predicted gene and the third most highly expressed gene *in vivo*. Remarkably, the
304 secretome expression pattern was completely different during growth on keratin, an *in vitro*
305 condition that was supposed to mimic the host environment (Fig. 6B, Fig. 3B and 3C). Only
306 five genes were found to be common to Tables 4A and 4B: two encoding putative GPI-
307 anchored proteins (ARB_01627 and ARB_07696), ARB_02741 encoding a CFEM domain
308 protein, ARB_06390 a putative cell wall protein, and ARB_02369 a carboxylesterase
309 domain-containing protein. This difference is even more striking when we focus our
310 analysis on secreted proteases. Even if about 20% of the 100 most expressed secreted
311 proteins are proteases in both *in vivo* and in keratin (Fig. 3B), the batch of proteins
312 expressed in these different conditions is clearly different (Fig. 3C). This is in accordance
313 with our above-mentioned WGCNA analysis in which relevant correlation groups were
314 found only when *in vivo* and keratin conditions were contrasted (Gp8+Gp14:Sa+S+K,
315 Gp8+Gp14+Sa:S+K, Gp8+Gp14+S:Sa+K, or Gp8+Gp14+Sa+S:K). Expression patterns in
316 soy and Sabouraud are closer to that in keratin, yet they are distinct from each other (see
317 Fig. 4), which explains their relatively neutral impact in the WGCNA contrasts.

318 Fig. S4 lists the 12 most highly expressed genes encoding proteases during infection
319 and those expressed on keratin. The genes encoding SUB6 (ARB_05307), SUB10
320 (ARB_06467), and the deuterolysin (ARB_04336) are highly and specifically upregulated
321 during the infection phase with fold changes of 2000x, 60x, and 100x, respectively. The
322 gene encoding SUB8 (ARB_00777) was relatively downregulated in keratin. PEP2
323 (ARB_02919), which is a putative ortholog of the vacuolar aspartic protease of *S.*
324 *cerevisiae* PrA and has been subsequently identified in other filamentous fungi, was found
325 to be highly expressed under all the *in vivo* and *in vitro* conditions.

On the other hand, the protease genes upregulated in keratin include subtilisins SUB3 (encoded by ARB_00701) and SUB4 (ARB_01032), the metallocarboxypeptidase MCPA of the M14 family (ARB_07026_07027), the leucine aminopeptidases LAP1 (ARB_03568) and LAP2 (ARB_00494), the aspartic protease OPSB (ARB_04170), and two extracellular metalloproteases (ARB_05085, ARB_05317).

Likewise, in the soy culture, only four protease genes were highly expressed: SUB4 (encoded by ARB_01032), LAP2 (ARB_00494), PEP2 (ARB_02919), and DPPV (ARB_06651) (Table S1). With the Sabouraud culture, in addition to PEP2, SUB8 (ARB_00777), OPSB (ARB_04170), DPPIV (ARB_06110) and a gene encoding an uncharacterized S10 family protease (ARB_01491) showed relatively high expression (Table S1).

DISCUSSION

Most previously available dermatophyte ORFs had been deduced by cDNA analysis and by expressed sequence tag sequencing using RNA extracted from dermatophytes grown *in vitro*. RNA-seq data obtained from *A. benhamiae* grown in various liquid culture conditions and most importantly during infection in guinea pigs led us to an improved gene prediction and annotation of its genome. A complete gene expression profile of *A. benhamiae* was obtained during infection of its natural host.

New *Arthroderma benhamiae* gene annotation

About 65% difference and, particularly, 383 new protein-coding genes were detected compared to the existing gene prediction. We used previously acquired MS data to validate *a posteriori* the presence of the predicted ORFs in culture supernatant. A comparable

approach with emphasis on proteogenomics has been recently used to review the genome and proteome of *T. rubrum* (21). In this study, the identification of 323 new peptides by MS in culture supernatant led to the refinement of 161 genes and the prediction of nine new genes. However, the RNA-seq analysis to validate the whole-genome proteomics was only performed with RNA extracted from *T. rubrum* cultured *in vitro* on potato glucose agar, but not during infection. This previous study and our results have in common the combination of experimental data with bioinformatics software and manual curation to generate an improved gene annotation. Our study focuses furthermore on the biology of infection.

In silico analysis of our predicted proteome led to the identification of 457 putative cell surface and secreted proteins. Our list of probable secreted proteins is likely to also contain proteins targeted to intracellular organelles, such as the endoplasmic reticulum or vacuole, since the exploited prediction tools cannot distinguish between such proteins and secreted ones. The Fungal Secretome and Subcellular Proteome KnowledgeBase (http://proteomics.ysu.edu/secretomes/fungi2/index.php) tries to address this concern by providing the prediction of secreted and organellar localization of proteins. It basically utilizes the same tools as we used in our strategy and reveals the same functional groups (22). In addition, they use WoLF PSORT (http://www.genscript.com/wolf-psort.html) that converts protein sequences into numerical localization features, based on sorting signals, amino acid composition and functional motifs. Nevertheless, this tool can produce a high number of false positives. Moreover, homologs of well-known intracellular proteins have been found in the secretome proteomic data. As an example, ARB_02919 is the closest *A. benhamiae* homolog of the *A. fumigatus* vacuolar aspartic peptidase (PEP2) and *S. cerevisiae* vacuolar proteinase A (PEP4). The latter is a vacuolar enzyme required for the

processing of vacuolar precursors (23), whereas the former plays an additional role linked to the cell wall (24). ARB_02919 was found as a secreted protein by MS (16), and is one of the most expressed proteins in all the five studied conditions. Contaminations cannot be ruled out, but our strategy ensures the best coverage of cell surface and secreted proteins, even if some false positives are probably still present.

Reprogramming of gene expression from a saprophyte to a parasite lifestyle

Striking differences were revealed between transcriptomes of *A. benhamiae* during growth under various conditions *in vitro* and during infection of its natural host. Such differences emphasize the importance of performing transcriptional analysis directly during infection, instead of using *in vitro* conditions that are expected to mimic the host environment. We also identified several newly predicted genes, as well as genes with unknown functions, that were differentially expressed in the contrast of *in vivo* versus *in vitro*, and, thus, might have a relevant role in infection. To sum up, the ability of dermatophytes to switch from a saprophyte to a parasite lifestyle is attested by an important reprogramming of gene expression.

Several comparative RNA-seq analyses were performed for other species of human pathogenic fungi (25–28), but as these studies rely on infection-mimicking conditions and not on the real *in vivo* situation, we think that they should be considered with caution. Only few studies were performed in real infection conditions. Gene expression profiles of *C. albicans* were obtained during infection in both the mouse kidney and the insect *Galleria mellonella* (29). Interestingly, gene expressions in these very distinct hosts were much closer to each other than in the *in vitro* liquid cultures used as controls. More recently, transcriptional profiling of *Blastomyces* was performed in co-cultures with human bone

marrow-derived macrophages and during *in vivo* pulmonary infection in a mouse model (30). They identified a number of functional categories upregulated exclusively *in vivo*, including secreted proteins, zinc acquisition proteins, as well as cysteine and tryptophan metabolism. Nine secreted protein were identified, including products of five of the ten most upregulated genes during infection. One of these genes, BDFG_00717, encodes a CFEM-domain-containing protein, highlighting the importance of those proteins in virulence.

Potential non-protease virulence factors of *Arthroderma benhamiae*

Numerous genes that were highly expressed during infection encode uncharacterized proteins. Highly expressed protein-coding genes with a putative function other than proteolysis included ARB_01183, encoding a putative antigenic thaumatin domain protein, and two genes encoding 1,3-beta-glucanosyltransferases (ARB_07487 and ARB_05770). ARB_01183 was the most expressed secreted protein-coding gene *in vivo*. Thaumatin-like proteins (TLPs) are found in many eukaryotes and have been particularly studied in plants, in which they are involved in defense against fungal pathogens. Plant TLPs also have been shown to act as important allergens (31). TLPs are also found in fungi, such as *Moniliophtora perniciosa*, and may be involved in the inhibition of growth of fungal competitors and pathogenicity (32). The 1,3-beta-glucanosyltransferases play an important role in fungal cell wall morphology and pathogenicity. Deletion of the gene *GEL*2 encoding a 1,3-beta-glucanosyltransferase in *A. fumigatus* leads to altered cell wall composition as well as to reduced virulence in a murine model of invasive aspergillosis (33). GAS1 of the entomopathogenic fungus *Beauveria bassiana* contributes similarly to its mycoinsecticide activity (34).

ARB_02741, like *Blastomyces* BDFG_00717, encodes a GPI-anchored CFEM domain protein which is highly expressed *in vivo* and *in vitro* conditions. Its function has not been characterized yet, but it is interesting to note that the closest homologs of ARB_02741 in the human fungal pathogen *Coccidioides posadasii* are the proline-rich antigens Ag2/PRA and Prp2, which have been reported to be leading vaccine candidates (35, 36). CFEM-domain proteins have been shown to be important for haem uptake and virulence in *C. albicans* (37). The ability to acquire iron from host tissues is a major virulence factor of pathogenic microorganisms. However, the exact implication of these proteins in infection processes is still unclear. As an example, the three *A. fumigatus* CFEM-domain proteins have been shown to be important for cell wall stability, not for virulence (38). Other proteins may also be involved in immune escape, such as ARB_06975, whose *A. fumigatus* hydrophobin homolog was shown to prevent immune recognition by forming a hydrophobic layer on the cell surface (39).

Arthroderma benhamiae **secreted proteases during infection**

SUB6 was the most highly expressed gene encoding a secreted protease during infection in guinea pigs. In addition to *SUB6*, other *A. benhamiae* protease genes encoding the subtilisins SUB7, SUB8, and SUB10 as well as a neutral protease of the deuterolysin family (M35) were also specifically upregulated. RNA-seq analysis results also confirmed that genes encoding major proteases secreted by the fungus during growth in a protein medium (i.e., SUB3, SUB4, MEP3, MEP4, LAP1, and DPPIV) were expressed at a relatively low level during infection as well as in Sabouraud medium and were not upregulated. These results are in accordance with recent findings by proteomic analysis (LC-MS/MS) in *T. rubrum*-infected nails that revealed SUB6 as the major protein secreted by the fungus in

onychomycosis (40). The closely related SUB7 (subtilisin-like protease 7, Q8NID9) and DPPV (dipeptidyl-peptidase 5, Q9UW98) were also detected. Likewise, most major proteases secreted by the fungus during its growth *in vitro* in a protein medium (11, 41) were not detected and, therefore, appeared not to be involved during the establishment of onychomycosis. As a general conclusion, the proteases secreted *in vitro* during protein degradation and *in vivo* during infection are different, regardless of the dermatophyte species and the *tinea*. The view that the proteases isolated from dermatophytes grown *in vitro* in a protein medium are virulence attributes and exert a major role during infection appears to be too naïve and can no longer be accepted. Dermatophytes evolved from soil saprophytic fungi that are able to efficiently degrade hard keratin into amino acids and into short peptides in the process of recycling nitrogen, and the pathogenic phase of dermatophytes has to be dissociated from their saprophytic phase. Some of the multiple members of protease gene families in dermatophytes are dedicated exclusively to protein degradation while others, such as SUB6, likely fulfill specific roles during infection. The notion that proteases secreted in proteinaceous media correspond to virulence attributes has also been discarded for other pathogenic fungi. Two different *A. fumigatus* mutants unable to secrete proteolytic activity in a protein growth medium did not show attenuated virulence when tested in a leukopenic mouse model. In the first mutant, the genes coding the two major secreted proteases ALP and MEP (42) were deleted. In the other mutant, the gene coding a transcriptional activator (PRTT) which regulates transcription of genes encoding the major proteases secreted in a protein medium was deleted. Noteworthily, no homolog of PRTT in *Aspergillus* spp. (43, 44) has been identified in *A. benhamiae*.

Genes encoding major proteases secreted by dermatophytes during *in vitro* growth in a

462 protein medium are tightly controlled by *DNR1*, the ortholog of *AREA* in *Aspergillus*
463 *nidulans* (45). In the absence of ammonium and glutamine, this transcription factor was
464 found to be required for the expression of genes involved in nitrogen metabolism. Although
465 dermatophytes infect keratinized tissues, our results suggest that the panel of proteases
466 secreted during infection depends on other transcription factors that remain to be
467 discovered.

468 ***Arthroderma benhamiae* secreted proteins as allergens**

469 Secreted proteins are allergens that play a key role in the pathogenic process. SUB6,
470 DPPV, and the beta-glucosidase ARB_05770 (encoded by three of the most expressed
471 genes of *A. benhamiae* during infection) are orthologs of the three known major
472 dermatophyte allergens Tri t1, Tri r2, and Tri r4, which are involved in bronchial
473 sensitization and symptomatic asthma (12, 46, 47). Dermatophyte antigens are also
474 involved in eczematous skin reactions at a location distant from the area of dermatophyte
475 infection (dermatophytids). The etiology of common dyshidrotic and vesicular eczema on
476 the hands (palms and fingers) is rarely investigated and may remain elusive because no
477 commercially standardized antigens are available to perform routine skin tests and antibody
478 detection. Trichophytin, a fungal extract that greatly varies in its preparation and
479 composition, was used to diagnose dermatophytids (48, 49). The secreted proteins
480 encoded by genes highly expressed during infection are the best candidates for the
481 detection of dermatophyte allergic diseases. At a time when quality in laboratory techniques
482 is a key issue, it would be relevant to perform skin test reactions using standardized
483 antigens in cases of eczematous skin reactions of unknown origin. A positive reaction could

be indicative of a non-detected dermatophyte infection and could suggest possible antifungal treatment.

Conclusion

Comparing gene expression during infection phase versus keratin degradation *in vitro* shows the importance of using real *in vivo* conditions to further investigate the virulence mechanisms of dermatophytes, instead of using some *in vitro* conditions supposed to mimic the host environment. Focusing our analysis on genes encoding cell-associated and secreted proteins, in particular proteases, led to the identification of strong candidates as allergens and putative virulence factors. The new genome annotation provided in this study might serve as a reference for annotation or re-annotation of other dermatophyte species and evolutionary related filamentous fungi.

MATERIALS AND METHODS

Strains and growth media

Arthroderma benhamiae Lau2354-2 (CBS 112371) (3, 50) was used in this study. This strain, deposited in the Belgian Coordinated Collections of Microorganisms (BCCM/IHEM) under IHEM20161, is the reference strain that was chosen for *A. benhamiae* genome sequencing (3). It was isolated from a patient suffering from a highly inflammatory dermatophytosis in the Centre Hospitalier Universitaire Vaudois (CHUV). The *A. benhamiae* strain was maintained at 28 °C on Sabouraud dextrose agar medium.

Arthroderma benhamiae was grown *in vitro* in Sabouraud liquid medium, soy protein liquid medium, and keratin liquid medium as previously described (7). Soy medium was prepared by dissolving 2 g of soy protein (Supro 1711, Protein Technologies International)

in 1 L of distilled water. Aliquots of 100 mL of keratin medium were prepared by adding 0.2 g of keratin (Merck, Darmstadt, Germany; keratin is derived from animal hooves and horns) and 5 mL of soy medium to 95 mL of distilled water. A low amount of soy protein in keratin liquid medium was found to be necessary to initiate the growth of dermatophytes with keratin as the sole substrate (7). A plug of fresh *A. benhamiae* mycelia grown on Sabouraud agar was inoculated in 100 mL of liquid Sabouraud, soy, and keratin medium and incubated for 5, 10 and 24 days, respectively, at 30 °C without shaking. At the indicated time points, growth in protein media was accompanied by substantial proteolytic activity along with clarification of the media and, in the case of keratin medium cultures, also by visible dissolution of the water-insoluble keratin granules.

Animal infection

Specific pathogen-free, 3-month-old female guinea pigs (cross-bred white albinos, Dunkin Hartley strain-Charles River Laboratories International, Wilmington, USA) were infected with *A. benhamiae* Lau2354-2. *Arthroderma benhamiae* mycelia scraped from freshly grown 18-day-old Sabouraud plates and suspended in 5% (w/w) poloxamer 407 (BASF, Germany) was applied to a 16-cm^2 back skin surface that had been clipped and scarified previously. Each guinea pig was infected with 6×10^9–2×10^{10} CFU. Non-infected control guinea pigs were subjected to the same procedure, except that the poloxamer 407 mixture did not contain any fungal elements. Three guinea pigs were sacrificed after 8, 14, 27, 44 days and 14 days after reinfection once healed. The infected skin from sacrificed animals was frozen at -80 °C for subsequent total RNA isolation. Both the hair and *stratum corneum* were examined for the presence of fungal elements by direct mycological examination.

Animal experiments were approved by the local ethics committee (University of Liège, ethics protocol no. 1052).

RNA extraction

RNA extraction from *A. benhamiae* cultures and infected guinea pig skin was performed using a specific procedure to yield sufficient amounts of quality RNA (see Supplementary Materials).

RNA sequencing

In close collaboration with the Lausanne Genomic Technologies Facility, and using the Illumina technology (HiSeq 2000 sequencer), we performed a TruSeq stranded single read total RNA analysis, using one lane with a multiplex level of 15, acquiring approximately 30 million 'strand-specific' reads with a length of 100 bp for each sample. Reads were aligned against the *A. benhamiae* and guinea pig genomes using *tophat2* (version 2.0.9) (51).

Strain and sequence data accession number

The genome assembly GCA_000151125.2 ASM15112v2 of *A. benhamiae* Lau2354-2 was used throughout this study. The raw RNA-seq data investigated here are accessible under the BioProject accession number SRP064455. The annotation is accessible under the BioSample accession number SAMN05163190. The CavPor3 draft assembly of the guinea pig genome was used.

Gene prediction and annotation

Gene prediction was made with *augustus* (version 3.0.2) (13) using a specific gene model obtained as follows. Gene transcripts and intron locations were obtained using *cufflinks* (version 2.2.1) (52). The transcripts were three-frame translated into potential amino-acid

sequences using *transeq* from EMBOSS (version 6.5.7) (53). The complete proteomes of *Saccharomyces cerevisiae* and *Aspergillus nidulans* (reviewed by Swiss-Prot) were mapped onto the potential amino acid sequences with *glsearch36*, from the FASTA alignment tools (version 3.6) (54) to identify coding phase and CDS location within transcripts. Based on the alignment quality and on the presence of start and stop codons near alignment extremities (+/- 10 amino acids), a set of confidently predicted CDS was gathered and converted into gene annotations using intron locations previously given by *cufflinks*. These annotations were used as a training set to build a gene model (available upon request) with the scripts supplied in the *augustus* distribution.

In silico identification of putative cell surface and secreted proteases

To identify putative secreted proteins, we checked for the presence of an N-terminal signal sequence using both *Phobius* (version 1.01) (55) and *SignalP* (version 4.1) (56). Signal peptides have been confirmed by the prediction of N-terminal transmembrane spans using *TMHMM* (version 2.0) (57, 58). The presence of a potential glycosylphosphatidylinositol (GPI) anchor has been checked by using *PredGPI* (version 1.0) (59). Using the transmembrane span predictors *TMHMM* (version 2.0), *ESKW* (version 1.0) (60), and *MEMSAT* (version 1.8) (61), we refined the secretome prediction by removing the proteins that contain one or more transmembrane spans in addition to the signal peptide and that are probably targeted to membranes. All the secreted proteins have been subjected to Blast analysis against the UniProtKB database (18) as well as to InterPro scanning (19, 20) to associate and reveal some putative functions.

Mass spectrometry and experimental validation of new secreted proteins

572 Precipitation and separation of proteins from *A. benhamiae* cultures at pH 4 and pH 7 along
573 with shotgun mass spectrometry (MS) experiments have been described by
574 Sriranganadane et al. (16). A new search of MS/MS spectra against the sequences of our
575 new predicted proteome was performed.

576 **Transcriptome analysis**

577 The number of reads mapped onto each newly predicted gene locus was obtained with
578 *htseq-count* (version 0.5.4p3) (62). Genes with counts fewer than one per million in all
579 samples were removed from the statistical analyses (i.e., 81 genes). Gene expression was
580 normalized using the TMM-normalized Voom transformation (63); hierarchical clustering
581 and principal component analysis was done using R (version 3.1.1). Differential gene
582 expression analysis was performed with the R Bioconductor package *limma* (64). The cut-
583 offs of 1e-3 for FDR (BY-adjusted *p*-value) (65) and 2 for fold change were applied to
584 identify genes relevant to each contrast. The R software package *WGCNA* (66) was used
585 for correlation network analysis, using the Pearson correlation.

586 **Pathway enrichment**

587 The predicted *A. benhamiae* proteins were aligned against *Saccharomyces cerevisiae*
588 proteins from Swiss-Prot with *inparanoid* (version 4.1) (67) to identify the orthologs from
589 which the Gene Ontology (GO) terms were extracted and applied to *A. benhamiae.* We
590 then performed the GO enrichment analysis on the weighted gene correlation network
591 analysis (WGCNA) gene modules.

592 ## ACKNOWLEDGEMENTS

593 This work was supported by the Swiss National Science Foundation grant 31003A_140514
594 to Michel Monod and Marco Pagni. It was also partly supported by grant 3.4558.10 from
595 Fonds de la Recherche Scientifique Médicale (FRSM, Belgium) and 594/2012 from the
596 Executive Unit for Higher Education, Research, Development and Innovation Funding
597 (UEFISCDI, Romania) to Bernard Mignon. E.T.B. was the recipient of a research grant
598 provided by the University of Liège and supported by the agreement that binds Wallonia-
599 Brussels (WBI) and Romania. The computations were performed at the Vital-IT Center for
600 high-performance computing (http://www.vital-it.ch) of the SIB Swiss Institute of
601 Bioinformatics. SIB receives financial supports from the Swiss Federal Government through
602 the State Secretariat for Education and Research. We thank Sandra Calderon for supports
603 in the RNA-seq analysis, and Edouard de Castro for supports in the signal peptide
604 prediction.

605

606 ## REFERENCES

607 1. **Weitzman I**, **Summerbell RC**. 1995. The dermatophytes. Clin Microbiol Rev **8**:240–
608 259.
609 2. **Degreef H**. 2008. Clinical forms of dermatophytosis (ringworm infection).
610 Mycopathologia **166**:257–265.
611 3. **Burmester A**, **Shelest E**, **Glöckner G**, **Heddergott C**, **Schindler S**, **Staib P**, **Heidel**
612 **A**, **Felder M**, **Petzold A**, **Szafranski K**, **Feuermann M**, **Pedruzzi I**, **Priebe S**, **Groth**
613 **M**, **Winkler R**, **Li W**, **Kniemeyer O**, **Schroeckh V**, **Hertweck C**, **Hube B**, **White TC**,
614 **Platzer M**, **Guthke R**, **Heitman J**, **Wöstemeyer J**, **Zipfel PF**, **Monod M**, **Brakhage**

AA. 2011. Comparative and functional genomics provide insights into the pathogenicity of dermatophytic fungi. Genome Biol **12**:R7.

4. **Martinez DA**, **Oliver BG**, **Gräser Y**, **Goldberg JM**, **Li W**, **Martinez-Rossi NM**, **Monod M**, **Shelest E**, **Barton RC**, **Birch E**, **Brakhage AA**, **Chen Z**, **Gurr SJ**, **Heiman D**, **Heitman J**, **Kosti I**, **Rossi A**, **Saif S**, **Samalova M**, **Saunders CW**, **Shea T**, **Summerbell RC**, **Xu J**, **Young S**, **Zeng Q**, **Birren BW**, **Cuomo CA**, **White TC**. 2012. Comparative genome analysis of Trichophyton rubrum and related dermatophytes reveals candidate genes involved in infection. mBio **3**:e00259–00212.
5. **Naglik JR**, **Challacombe SJ**, **Hube B**. 2003. Candida albicans secreted aspartyl proteinases in virulence and pathogenesis. Microbiol Mol Biol Rev MMBR **67**:400–428, table of contents.
6. **Lo Presti L**, **Lanver D**, **Schweizer G**, **Tanaka S**, **Liang L**, **Tollot M**, **Zuccaro A**, **Reissmann S**, **Kahmann R**. 2015. Fungal effectors and plant susceptibility. Annu Rev Plant Biol **66**:513–545.
7. **Staib P**, **Zaugg C**, **Mignon B**, **Weber J**, **Grumbt M**, **Pradervand S**, **Harshman K**, **Monod M**. 2010. Differential gene expression in the pathogenic dermatophyte Arthroderma benhamiae in vitro versus during infection. Microbiol Read Engl **156**:884–895.
8. **Jousson O**, **Léchenne B**, **Bontems O**, **Capoccia S**, **Mignon B**, **Barblan J**, **Quadroni M**, **Monod M**. 2004. Multiplication of an ancestral gene encoding secreted fungalysin preceded species differentiation in the dermatophytes Trichophyton and Microsporum. Microbiol Read Engl **150**:301–310.

9. **Jousson O**, **Léchenne B**, **Bontems O**, **Mignon B**, **Reichard U**, **Barblan J**, **Quadroni M**, **Monod M**. 2004. Secreted subtilisin gene family in Trichophyton rubrum. Gene **339**:79–88.

10. **Monod M**, **Léchenne B**, **Jousson O**, **Grand D**, **Zaugg C**, **Stöcklin R**, **Grouzmann E**. 2005. Aminopeptidases and dipeptidyl-peptidases secreted by the dermatophyte Trichophyton rubrum. Microbiol Read Engl **151**:145–155.

11. **Zaugg C**, **Jousson O**, **Léchenne B**, **Staib P**, **Monod M**. 2008. Trichophyton rubrum secreted and membrane-associated carboxypeptidases. Int J Med Microbiol IJMM **298**:669–682.

12. **Woodfolk JA**, **Wheatley LM**, **Piyasena RV**, **Benjamin DC**, **Platts-Mills TA**. 1998. Trichophyton antigens associated with IgE antibodies and delayed type hypersensitivity. Sequence homology to two families of serine proteinases. J Biol Chem **273**:29489–29496.

13. **Stanke M**. 2004. Gene prediction with a hidden markov model. University of Göttingen, Germany.

14. **Starck SR**, **Jiang V**, **Pavon-Eternod M**, **Prasad S**, **McCarthy B**, **Pan T**, **Shastri N**. 2012. Leucine-tRNA Initiates at CUG Start Codons for Protein Synthesis and Presentation by MHC Class I. Science **336**:1719–1723.

15. **Ehlers MR**, **Riordan JF**. 1991. Membrane proteins with soluble counterparts: role of proteolysis in the release of transmembrane proteins. Biochemistry (Mosc) **30**:10065–10074.

16. **Sriranganadane D**, **Waridel P**, **Salamin K**, **Feuermann M**, **Mignon B**, **Staib P**, **Neuhaus J-M**, **Quadroni M**, **Monod M**. 2011. Identification of novel secreted

proteases during extracellular proteolysis by dermatophytes at acidic pH. Proteomics **11**:4422–4433.

17. **Heddergott C**, **Bruns S**, **Nietzsche S**, **Leonhardt I**, **Kurzai O**, **Kniemeyer O**, **Brakhage AA**. 2012. The Arthroderma benhamiae hydrophobin HypA mediates hydrophobicity and influences recognition by human immune effector cells. Eukaryot Cell **11**:673–682.
18. **UniProt Consortium**. 2015. UniProt: a hub for protein information. Nucleic Acids Res **43**:D204–212.
19. **Quevillon E**, **Silventoinen V**, **Pillai S**, **Harte N**, **Mulder N**, **Apweiler R**, **Lopez R**. 2005. InterProScan: protein domains identifier. Nucleic Acids Res **33**:W116–120.
20. **Zdobnov EM**, **Apweiler R**. 2001. InterProScan--an integration platform for the signature-recognition methods in InterPro. Bioinforma Oxf Engl **17**:847–848.
21. **Xu X**, **Liu T**, **Ren X**, **Liu B**, **Yang J**, **Chen L**, **Wei C**, **Zheng J**, **Dong J**, **Sun L**, **Zhu Y**, **Jin Q**. 2015. Proteogenomic Analysis of Trichophyton rubrum Aided by RNA Sequencing. J Proteome Res **14**:2207–2218.
22. **Meinken J**, **Asch DK**, **Neizer-Ashun KA**, **Chang G-H**, **Cooper JR 4**, **Min XJ**. 2014. FunSecKB2: a fungal protein subcellular location knowledgebase. Comput Mol Biol **4**.
23. **Ammerer G**, **Hunter CP**, **Rothman JH**, **Saari GC**, **Valls LA**, **Stevens TH**. 1986. PEP4 gene of Saccharomyces cerevisiae encodes proteinase A, a vacuolar enzyme required for processing of vacuolar precursors. Mol Cell Biol **6**:2490–2499.
24. **Reichard U**, **Monod M**, **Odds F**, **Rüchel R**. 1997. Virulence of an aspergillopepsin-deficient mutant of Aspergillus fumigatus and evidence for another aspartic proteinase

linked to the fungal cell wall. J Med Vet Mycol Bi-Mon Publ Int Soc Hum Anim Mycol **35**:189–196.

25. **Irmer H**, **Tarazona S**, **Sasse C**, **Olbermann P**, **Loeffler J**, **Krappmann S**, **Conesa A**, **Braus GH**. 2015. RNAseq analysis of Aspergillus fumigatus in blood reveals a just wait and see resting stage behavior. BMC Genomics **16**:640.
26. **Chen F**, **Zhang C**, **Jia X**, **Wang S**, **Wang J**, **Chen Y**, **Zhao J**, **Tian S**, **Han X**, **Han L**. 2015. Transcriptome Profiles of Human Lung Epithelial Cells A549 Interacting with Aspergillus fumigatus by RNA-Seq. PloS One **10**:e0135720.
27. **Muszkieta L**, **Beauvais A**, **Pähtz V**, **Gibbons JG**, **Anton Leberre V**, **Beau R**, **Shibuya K**, **Rokas A**, **Francois JM**, **Kniemeyer O**, **Brakhage AA**, **Latgé JP**. 2013. Investigation of Aspergillus fumigatus biofilm formation by various “omics” approaches. Front Microbiol **4**:13.
28. **Edwards JA**, **Chen C**, **Kemski MM**, **Hu J**, **Mitchell TK**, **Rappleye CA**. 2013. Histoplasma yeast and mycelial transcriptomes reveal pathogenic-phase and lineage-specific gene expression profiles. BMC Genomics **14**:695.
29. **Amorim-Vaz S**, **Tran VDT**, **Pradervand S**, **Pagni M**, **Coste AT**, **Sanglard D**. 2015. RNA Enrichment Method for Quantitative Transcriptional Analysis of Pathogens In Vivo Applied to the Fungus Candida albicans. mBio **6**:e00942–00915.
30. **Muñoz JF**, **Gauthier GM**, **Desjardins CA**, **Gallo JE**, **Holder J**, **Sullivan TD**, **Marty AJ**, **Carmen JC**, **Chen Z**, **Ding L**, **Gujja S**, **Magrini V**, **Misas E**, **Mitreva M**, **Priest M**, **Saif S**, **Whiston EA**, **Young S**, **Zeng Q**, **Goldman WE**, **Mardis ER**, **Taylor JW**, **McEwen JG**, **Clay OK**, **Klein BS**, **Cuomo CA**. 2015. The Dynamic Genome and

Transcriptome of the Human Fungal Pathogen Blastomyces and Close Relative Emmonsia. PLoS Genet **11**:e1005493.

31. **Palacín A**, **Rivas LA**, **Gómez-Casado C**, **Aguirre J**, **Tordesillas L**, **Bartra J**, **Blanco C**, **Carrillo T**, **Cuesta-Herranz J**, **Bonny JAC**, **Flores E**, **García-Alvarez-Eire MG**, **García-Nuñez I**, **Fernández FJ**, **Gamboa P**, **Muñoz R**, **Sánchez-Monge R**, **Torres M**, **Losada SV**, **Villalba M**, **Vega F**, **Parro V**, **Blanca M**, **Salcedo G**, **Díaz-Perales A**. 2012. The involvement of thaumatin-like proteins in plant food cross-reactivity: a multicenter study using a specific protein microarray. PloS One **7**:e44088.

32. **Franco S de F**, **Baroni RM**, **Carazzolle MF**, **Teixeira PJPL**, **Reis O**, **Pereira GAG**, **Mondego JMC**. 2015. Genomic analyses and expression evaluation of thaumatin-like gene family in the cacao fungal pathogen Moniliophthora perniciosa. Biochem Biophys Res Commun **466**:629–636.

33. **Mouyna I**, **Morelle W**, **Vai M**, **Monod M**, **Léchenne B**, **Fontaine T**, **Beauvais A**, **Sarfati J**, **Prévost M-C**, **Henry C**, **Latgé J-P**. 2005. Deletion of GEL2 encoding for a beta(1-3)glucanosyltransferase affects morphogenesis and virulence in Aspergillus fumigatus. Mol Microbiol **56**:1675–1688.

34. **Zhang S**, **Xia Y**, **Keyhani NO**. 2011. Contribution of the gas1 gene of the entomopathogenic fungus Beauveria bassiana, encoding a putative glycosylphosphatidylinositol-anchored beta-1,3-glucanosyltransferase, to conidial thermotolerance and virulence. Appl Environ Microbiol **77**:2676–2684.

35. **Cox RA**, **Magee DM**. 2004. Coccidioidomycosis: host response and vaccine development. Clin Microbiol Rev **17**:804–839, table of contents.

36. **Herr RA**, **Hung C-Y**, **Cole GT**. 2007. Evaluation of two homologous proline-rich proteins of Coccidioides posadasii as candidate vaccines against coccidioidomycosis. Infect Immun **75**:5777–5787.

37. **Weissman Z**, **Kornitzer D**. 2004. A family of Candida cell surface haem-binding proteins involved in haemin and haemoglobin-iron utilization. Mol Microbiol **53**:1209–1220.

38. **Vaknin Y**, **Shadkchan Y**, **Levdansky E**, **Morozov M**, **Romano J**, **Osherov N**. 2014. The three Aspergillus fumigatus CFEM-domain GPI-anchored proteins (CfmA-C) affect cell-wall stability but do not play a role in fungal virulence. Fungal Genet Biol FG B **63**:55–64.

39. **Aimanianda V**, **Bayry J**, **Bozza S**, **Kniemeyer O**, **Perruccio K**, **Elluru SR**, **Clavaud C**, **Paris S**, **Brakhage AA**, **Kaveri SV**, **Romani L**, **Latgé J-P**. 2009. Surface hydrophobin prevents immune recognition of airborne fungal spores. Nature **460**:1117–1121.

40. **Méhul B**, **Gu Z**, **Jomard A**, **Laffet G**, **Feuilhade M**, **Monod M**. 2015. Sub6 (Tri r 2), an Onychomycosis Marker Revealed by Proteomics Analysis of Trichophyton rubrum Secreted Proteins in Patient Nail Samples. J Invest Dermatol.

41. **Giddey K**, **Monod M**, **Barblan J**, **Potts A**, **Waridel P**, **Zaugg C**, **Quadroni M**. 2007. Comprehensive analysis of proteins secreted by Trichophyton rubrum and Trichophyton violaceum under in vitro conditions. J Proteome Res **6**:3081–3092.

42. **Jaton-Ogay K**, **Paris S**, **Huerre M**, **Quadroni M**, **Falchetto R**, **Togni G**, **Latgé JP**, **Monod M**. 1994. Cloning and disruption of the gene encoding an extracellular metalloprotease of Aspergillus fumigatus. Mol Microbiol **14**:917–928.

43. **Punt PJ**, **Schuren FHJ**, **Lehmbeck J**, **Christensen T**, **Hjort C**, **van den Hondel CAMJJ**. 2008. Characterization of the Aspergillus niger prtT, a unique regulator of extracellular protease encoding genes. Fungal Genet Biol FG B **45**:1591–1599.

44. **Bergmann A**, **Hartmann T**, **Cairns T**, **Bignell EM**, **Krappmann S**. 2009. A regulator of Aspergillus fumigatus extracellular proteolytic activity is dispensable for virulence. Infect Immun **77**:4041–4050.

45. **Yamada T**, **Makimura K**, **Abe S**. 2006. Isolation, characterization, and disruption of dnr1, the areA/nit-2-like nitrogen regulatory gene of the zoophilic dermatophyte, Microsporum canis. Med Mycol **44**:243–252.

46. **Deuell B**, **Arruda LK**, **Hayden ML**, **Chapman MD**, **Platts-Mills TA**. 1991. Trichophyton tonsurans allergen. I. Characterization of a protein that causes immediate but not delayed hypersensitivity. J Immunol Baltim Md 1950 **147**:96–101.

47. **Woodfolk JA**. 2005. Allergy and dermatophytes. Clin Microbiol Rev **18**:30–43.

48. **Grappel SF**, **Bishop CT**, **Blank F**. 1974. Immunology of dermatophytes and dermatophytosis. Bacteriol Rev **38**:222–250.

49. **Ilkit M**, **Durdu M**, **Karakaş M**. 2012. Cutaneous id reactions: a comprehensive review of clinical manifestations, epidemiology, etiology, and management. Crit Rev Microbiol **38**:191–202.

50. **Fumeaux J**, **Mock M**, **Ninet B**, **Jan I**, **Bontems O**, **Léchenne B**, **Lew D**, **Panizzon RG**, **Jousson O**, **Monod M**. 2004. First report of Arthroderma benhamiae in Switzerland. Dermatol Basel Switz **208**:244–250.

770 51. **Kim D**, **Pertea G**, **Trapnell C**, **Pimentel H**, **Kelley R**, **Salzberg SL**. 2013. TopHat2:
771 accurate alignment of transcriptomes in the presence of insertions, deletions and gene
772 fusions. Genome Biol **14**:R36.
773 52. **Trapnell C**, **Roberts A**, **Goff L**, **Pertea G**, **Kim D**, **Kelley DR**, **Pimentel H**, **Salzberg**
774 **SL**, **Rinn JL**, **Pachter L**. 2012. Differential gene and transcript expression analysis of
775 RNA-seq experiments with TopHat and Cufflinks. Nat Protoc **7**:562–578.
776 53. **Rice P**, **Longden I**, **Bleasby A**. 2000. EMBOSS: the European Molecular Biology
777 Open Software Suite. Trends Genet TIG **16**:276–277.
778 54. **Pearson WR**. 1991. Searching protein sequence libraries: comparison of the
779 sensitivity and selectivity of the Smith-Waterman and FASTA algorithms. Genomics
780 **11**:635–650.
781 55. **Käll L**, **Krogh A**, **Sonnhammer ELL**. 2004. A combined transmembrane topology and
782 signal peptide prediction method. J Mol Biol **338**:1027–1036.
783 56. **Petersen TN**, **Brunak S**, **von Heijne G**, **Nielsen H**. 2011. SignalP 4.0: discriminating
784 signal peptides from transmembrane regions. Nat Methods **8**:785–786.
785 57. **Sonnhammer EL**, **von Heijne G**, **Krogh A**. 1998. A hidden Markov model for
786 predicting transmembrane helices in protein sequences. Proc Int Conf Intell Syst Mol
787 Biol ISMB Int Conf Intell Syst Mol Biol **6**:175–182.
788 58. **Krogh A**, **Larsson B**, **von Heijne G**, **Sonnhammer EL**. 2001. Predicting
789 transmembrane protein topology with a hidden Markov model: application to complete
790 genomes. J Mol Biol **305**:567–580.
791 59. **Pierleoni A**, **Martelli P**, **Casadio R**. 2008. PredGPI: a GPI-anchor predictor. BMC
792 Bioinformatics **9**:392.

60. **Eisenberg D**, **Schwarz E**, **Komaromy M**, **Wall R**. 1984. Analysis of membrane and surface protein sequences with the hydrophobic moment plot. J Mol Biol **179**:125–142.

61. **Jones DT**, **Taylor WR**, **Thornton JM**. 1994. A model recognition approach to the prediction of all-helical membrane protein structure and topology. Biochemistry (Mosc) **33**:3038–3049.

62. **Anders S**, **Pyl PT**, **Huber W**. 2015. HTSeq--a Python framework to work with high-throughput sequencing data. Bioinforma Oxf Engl **31**:166–169.

63. **Law CW**, **Chen Y**, **Shi W**, **Smyth GK**. 2014. voom: precision weights unlock linear model analysis tools for RNA-seq read counts. Genome Biol **15**:R29.

64. **Smyth GK**. 2005. limma: Linear Models for Microarray Data, p. 397–420. *In* Gentleman, R, Carey, VJ, Huber, W, Irizarry, RA, Dudoit, S (eds.), Bioinformatics and Computational Biology Solutions Using R and Bioconductor. Springer New York.

65. **Benjamini Y**, **Yekutieli D**. 2001. The Control of the False Discovery Rate in Multiple Testing under Dependency. Ann Stat **29**:1165–1188.

66. **Langfelder P**, **Horvath S**. 2008. WGCNA: an R package for weighted correlation network analysis. BMC Bioinformatics **9**:559.

67. **O'Brien KP**, **Remm M**, **Sonnhammer ELL**. 2005. Inparanoid: a comprehensive database of eukaryotic orthologs. Nucleic Acids Res **33**:D476–D480.

TABLES

TABLE 1 RNA-seq data summary

Library	Total cleaned reads (M*)	Aligned to *A. benhamiae* # reads	Aligned to *A. benhamiae* %	Aligned to *C. porcellus* # reads (M)	Aligned to *C. porcellus* %
8 dpi	34.5	0.5 M	1.5	31.8	92.3
	31.7	1 M	3.3	28.9	91.0
	26	1 M	4	23.5	90.6
14 dpi	31.8	44.5 K*	0.1	30	94.3
	30.6	51.2 K	0.2	28.9	94.4
	31.4	24.8 K	0.1	29.5	93.8
27 dpi	33.8	623	0	31.6	93.5
	39	657	0	36.6	94.0
	30.8	452	0	28.8	93.3
44 dpi	35.7	458	0	33.1	92.9
	31.9	857	0	29.6	92.7
	25.3	808	0	23.5	92.8
Control	26.1	637	0	24.3	93.4
	38.9	840	0	36.3	93.3
	35.7	3143	0	33.2	93.0
Keratin	12.4	6.1 M	49.2		
	13.5	7.9 M	58.3		
	13.9	8 M	57.6		
Soy	11.7	7.3 M	62.6		
	10.5	6 M	57.1		
	12.8	7.5 M	58.8		
Sabouraud	12.4	7.9 M	63.5		
	14.8	8.7 M	59.1		
	11.6	7.2 M	61.6		

* M, million; K, thousand.

TABLE 2 Comparison between the new gene set and the original one. *Matched*: identical old and new gene annotations; *Alternative*: conserved start and stop codons but different splicing; *Different*: different start or stop codons, possibly different splicing;

Merged: more than one old gene merged into a single new one; *Split*: old gene split into several new ones; *New*: genes only found in the new predictions (708 original genes were lost). *Auto*: gene annotations as produced by *augustus*; *Manual*: manual correction of the start codon. The number of genes whose products were confirmed by mass spectrometry in culture supernatants is given between parentheses. GPI: Glycosylphosphatidylinositol.

New vs old gene prediction	Gene count in complete genome	Gene count in secretome only							
		With GPI				Without GPI			
		Auto		Manual		Auto		Manual	
Matched	2662	47	(**13**)	2	(**2**)	155	(**55**)	0	
Alternative	1246	19	(**6**)	0		49	(**19**)	1	
Different	2752	31	(**6**)	1		83	(**19**)	10	(**4**)
Merged	286	5	(**2**)	0		7	(**2**)	1	
Split	76	1	(**1**)	0		5	(**2**)	0	
New	383	6		0		34	(**8**)	0	
	7405	109	(**28**)	3	(**2**)	333	(**105**)	12	(**4**)

TABLE 3 Designation of samples and growth conditions

RNA sample	Growth condition	
	Code	Description
Cb1	Gp8	*In vivo*: Guinea pig 8 days post infection
Cb2		
Cb3		
Cb4	Gp14	*In vivo*: Guinea pig 14 days post infection
Cb5		
Cb6		
K1	K	*In vitro*: Keratin medium
K2		
K3		

S1	S	*In vitro*: Soy medium
S2		
S4		
Sa1	Sa	*In vitro*: Sabouraud medium
Sa2		
Sa3		

828

829

830 ## FIGURES

831 **FIG 1 Experimental infection of the natural host of *Arthroderma benhamiae*.**

832 Cutaneously infected guinea pigs developed skin symptoms that were the most severe on

833 day 14 post infection (dpi) due to inflammation, while 8 dpi was the time point for the peak

834 of infection.

835 **FIG 2 Prediction and manual correction of the gene coding for the autophagy protein**

836 **Atg27 (ARB_01857: a trans-membrane protein).** (**A**) original gene prediction; (**B**)

837 automatic prediction from *augustus* (signal peptide is missing); (**C**) final (new) gene

838 prediction after manual correction. The re-annotation of this particular gene is remarkable,

839 as it produced a new intron, an alternative stop codon and a manually corrected start

840 codon.

841 **FIG 3 Characterization of the secretome. (A)** Pie chart showing the main functional

842 groups identified within the 457 proteins of the secretome. See detailed description in

843 Supplementary Results. **(B)** Pie charts showing the same functional groups as in **A**, but

844 within the 100 most expressed genes in Gp8 (*in vivo* 8 dpi), K (*in vitro* in keratin medium),

845 and S (*in vitro* in soy medium). **(C)** Venn diagram of proteases (top) and carbohydrate/cell

846 wall metabolism proteins (bottom) present in the 100 most expressed secreted proteins in

847 the 3 conditions described in **B**. Proteases represent about 20% of the 100 most expressed

proteins in the 3 conditions, however, the batch of proteins is clearly different in Gp8 when compared to K and S. This trend is not as significant when comparing carbohydrate/cell wall metabolism proteins.

FIG 4 Hierarchical clustering (A, C) and principal component analysis (B, D) of RNA sequencing samples considering the genes from the complete genome (A, B) or only the secretome subset (C, D). The sample names reflect the growth conditions: Cb, *in vivo* in guinea pig; S, *in vitro* in soy medium; Sa, *in vitro* in Sabouraud medium; K, *in vitro* in keratin medium. The *in vivo* samples cluster together.

FIG 5 Number of differentially expressed genes versus the enumeration of all possible contrasting conditions in the genome and the secretome, using a cut-off of 1e-3 for FDR and 2 for the fold change.

FIG 6 (A) Twenty-five most highly expressed genes encoding secreted proteins during infection compared to *in vitro* expression; **(B) Twenty-five most highly expressed genes encoding secreted proteins *in vitro* (keratin medium) compared to *in vivo* expression.**

SUPPLEMENTARY TABLES

TABLE S1 The secretome: predicted cell surface/secreted proteins, putative functions, and expression

[1] Open reading frame (ORF) names in this study

[2] The status indicates the changes between previous proteome annotation and our predictions

[3] ORF names in the previous genome annotation (Burmester et al. 2011)

[4] Names attributed to some proteases by Burmester et al. (2011) and Sriranganadane et al. (2011)

[5] UniProt accession numbers corresponding to the previous prediction. When two ORFs have been merged in the new prediction and both are present in UniProtKB, the two corresponding ACs are indicated.

[6] The presence of a signal peptide is indicated by SIG. SIG + GPI indicates that the gene product is predicted to have a GPI anchor.

[7] Mass spectrometry data were extracted from Sriranganadane et al. (2011). For each identified gene product, we indicate the medium pH in which it was detected (either pH 4 or 7).

[8] Function has been assigned based on homology search in well-characterized fungi and/or from InterPro scanning to identify specific domains and families. Green identifies proteins with a potential role in proteolytic activity; red, proteins involved in carbohydrate metabolism; and orange, proteins involved in lipid metabolism.

[9] Homologous fungal allergens extracted from the Allergome database (http://www.allergome.org/)

[10] Name of weighted gene correlation network analysis (WGCNA) gene co-expression module

[11] Summary of differential gene expression *in vivo* versus *in vitro*. Cut-offs: FDR = 1e-3 and 2-fold change.

[12] Significant expression trends from RNA sequencing data are indicated. The cut-off of -1 for the *z*-score of transcripts per million was applied.

[13] Mean expression values expressed in transcripts per million for every growth condition. The detailed counts per sample are given in Table S3.

TABLE S2 Potential allergens based on sequence homology

[1] Open reading frame (ORF) names in this study that have homologues acting as allergens in other fungi (and wasp in the case of ARB_02861).

[2] Allergens were retrieved from the Allergome database (http://www.allergome.org/).

[3] The (+) indicates *A. benhamiae* allergen homologs identified as encoding putative cell surface/secreted proteins in our study.

[4] Function has been assigned based on homology search in well-characterized fungi and/or from InterPro scanning to identify specific domains and families.

TABLE S3 Detailed counts per sample, differential expression, and weighted gene correlation network analysis module attribution

TABLE S4 Pathway enrichment analysis of weighted gene correlation network analysis modules. Only the most significant Gene Ontology terms are reported.

SUPPLEMENTARY FIGURES

FIG S1 Manual curation on SUB10 and SED3.

Actual and previous open reading frame predictions for SUB10 (A) and SED3 (B). N-terminal signal peptides, pro-peptides and peptidase domains are illustrated with boxes of different hues. The correction of assembly errors in actual open reading frames are indicated in red. Full ORFs were restored by the manual addition of the missing T in the SUB10 DNA sequence and G in the SED3 DNA sequence. These corrections have been confirmed by Sanger re-sequencing. The actual protein sequences of SUB10 and SED3 are available on the UniProtKB database (http://www.uniprot.org/) with respective accession numbers D4AQG0 and D4AK75.

FIG S2 Module-contrast correlations

FIG S3 Heatmap of the (A) turquoise module; (B) blue module; (C) tan module; (D) midnightblue module; (E) yellow module

FIG S4 Twelve most highly expressed genes encoding secreted proteases during infection (left table) and during *in vitro* growing in keratin medium (right table).

FIG S5 Quality of RNA extracted using the QIAGEN RNA extraction kit (A) and the protocol described in material and method section (B). The 18s rRNA and 28s rRNA absorbance peaks are shown in purple and blue, respectively.

SUPPLEMENTARY MATERIALS AND RESULTS

Supplementary.pdf

0 dpi

8 dpi

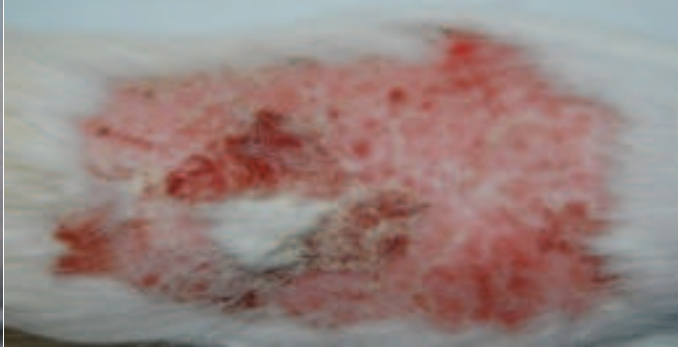

14 dpi

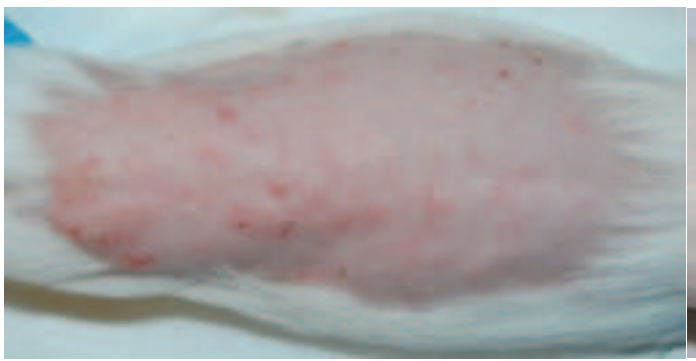

27 dpi

44 dpi

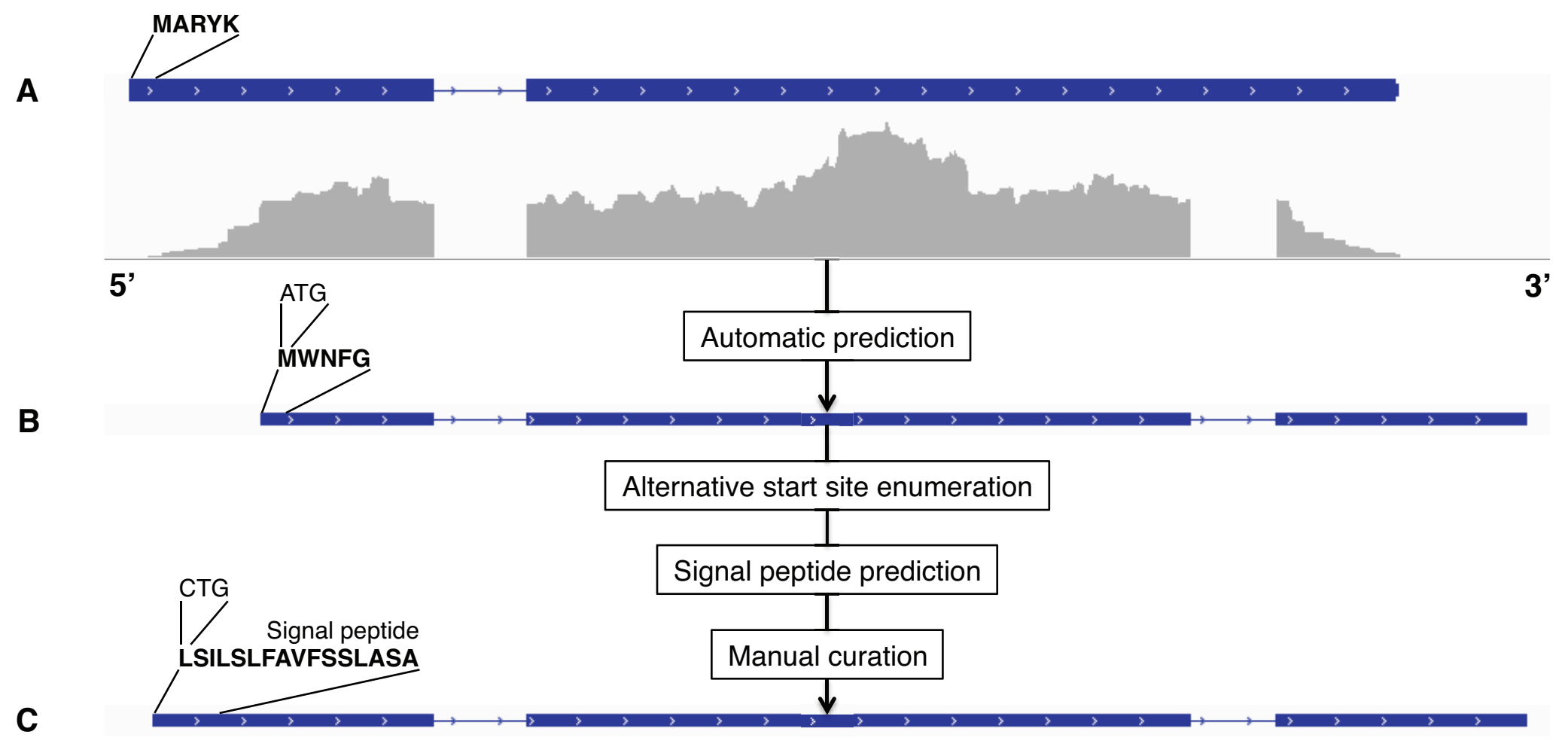
MARYK
A
5’
3’
ATG
MWNFG
B
Automatic prediction
Alternative start site enumeration
Signal peptide prediction
Manual curation
CTG
Signal peptide
LSILSLFAVFSSLASA
C

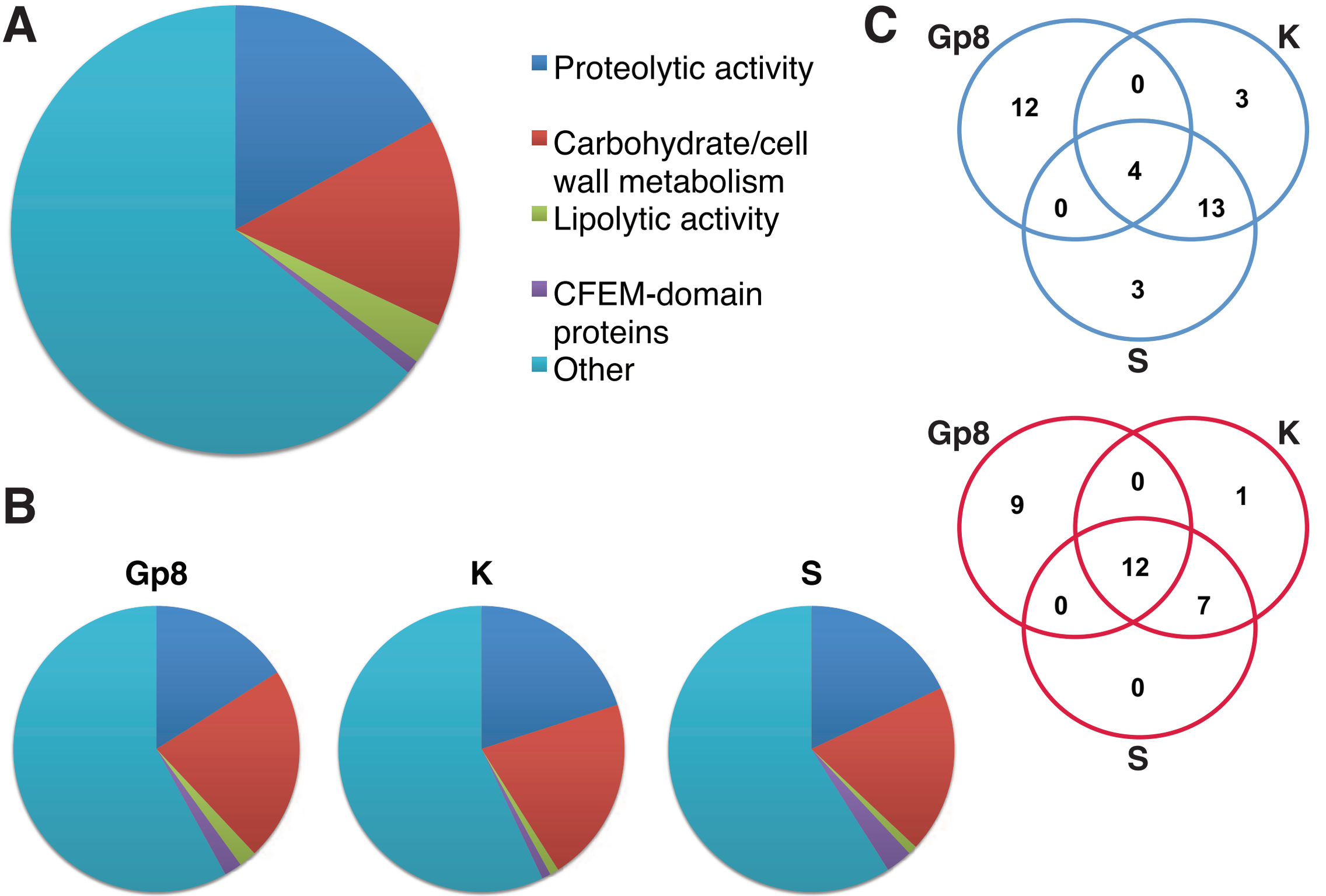
A
Proteolytic activity
Carbohydrate/cell wall metabolism
Lipolytic activity
CFEM-domain proteins
Other
B
Gp8
K
S
C
Gp8
K
S
12
0
3
4
0
13
3
Gp8
K
S
9
0
1
12
0
7
0

Genome

A

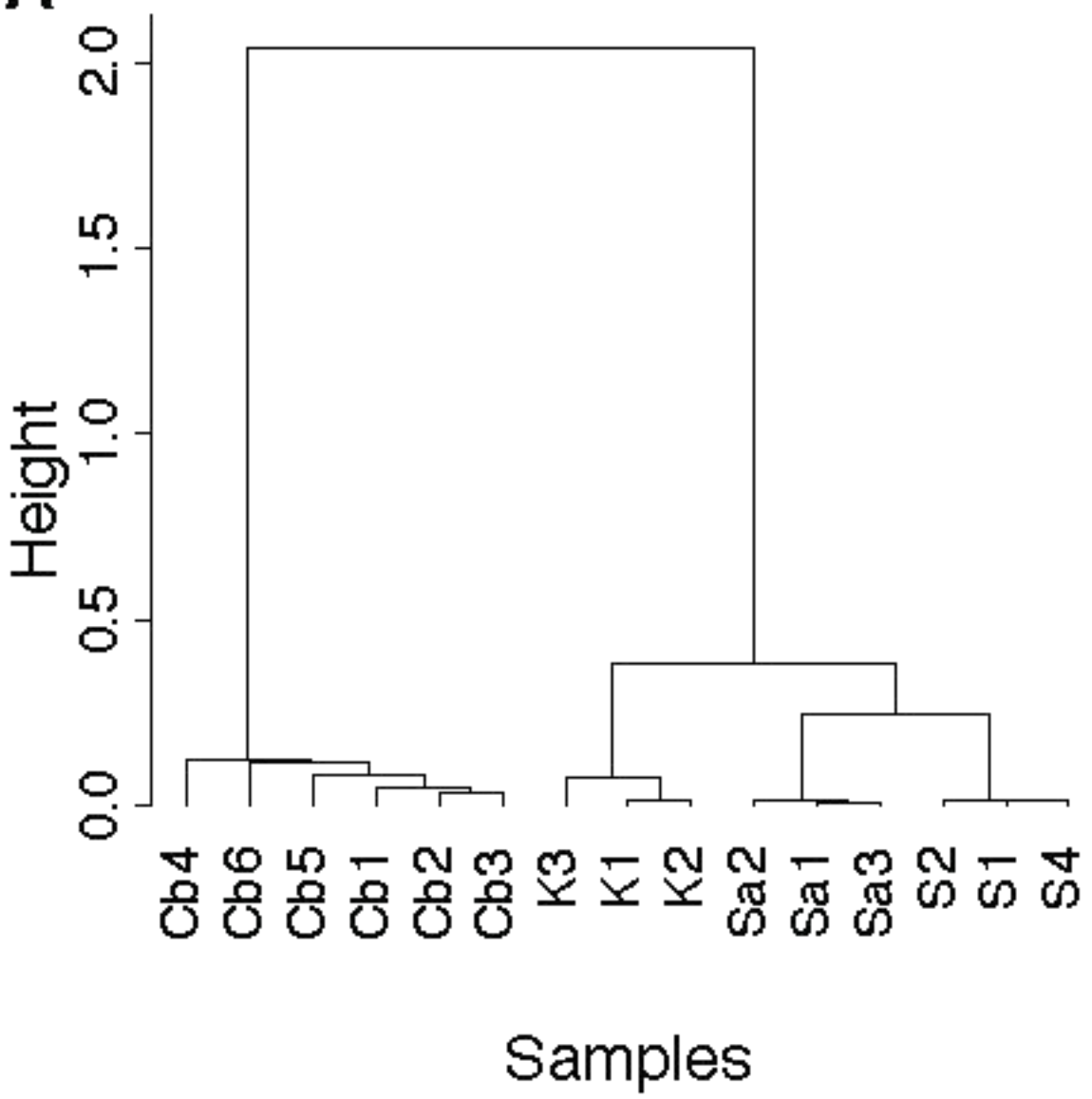

B

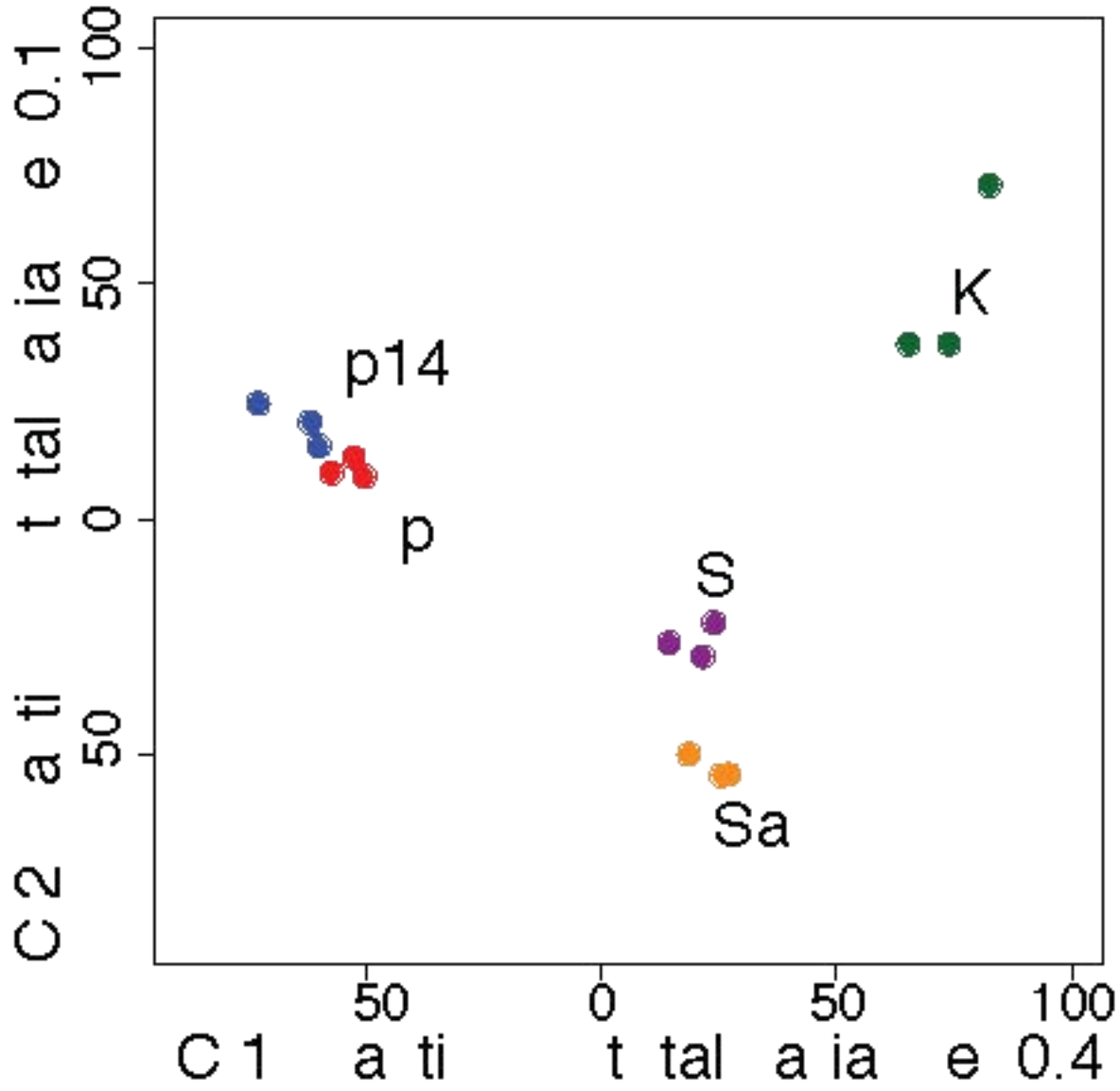

e e ome

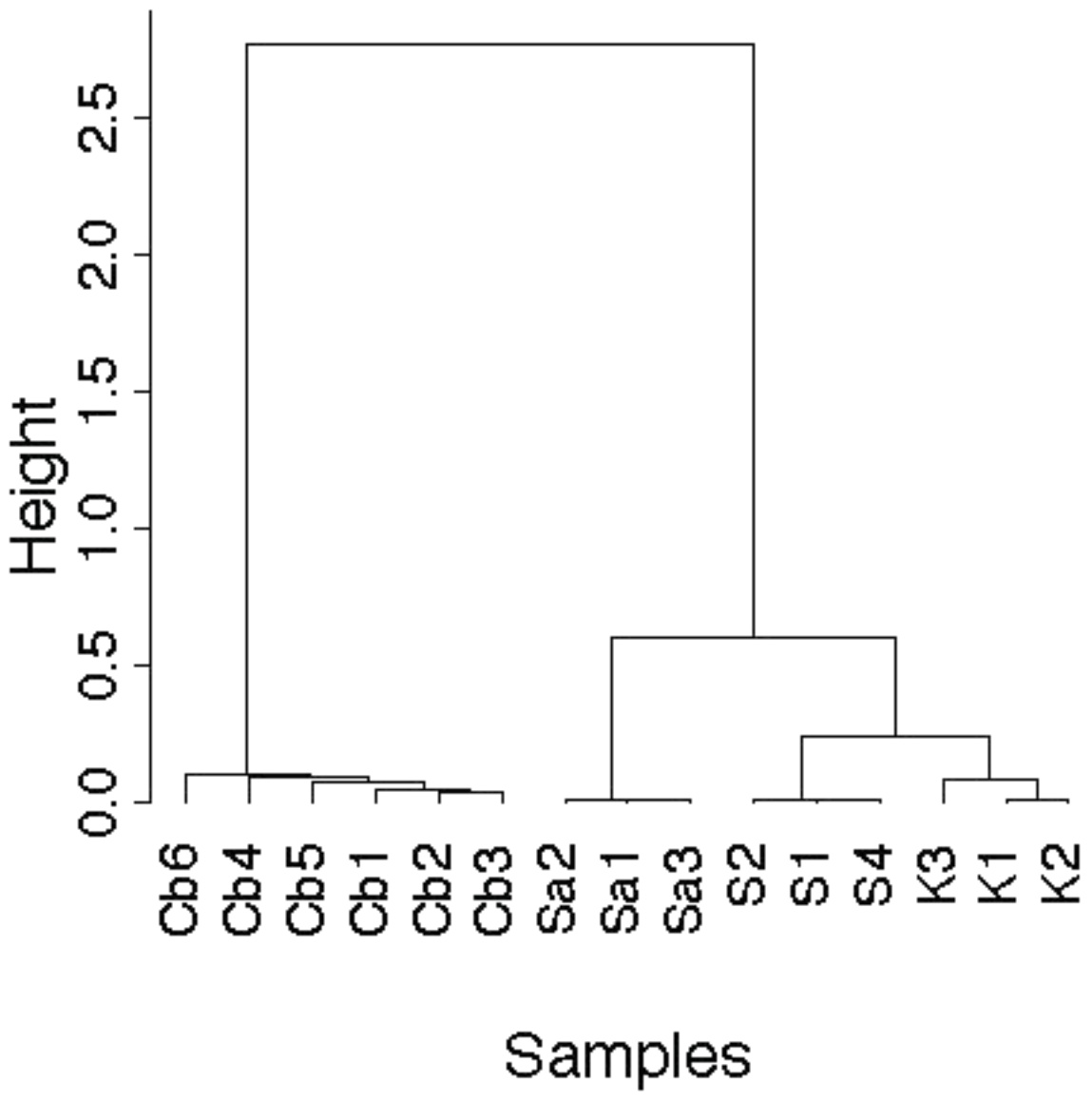

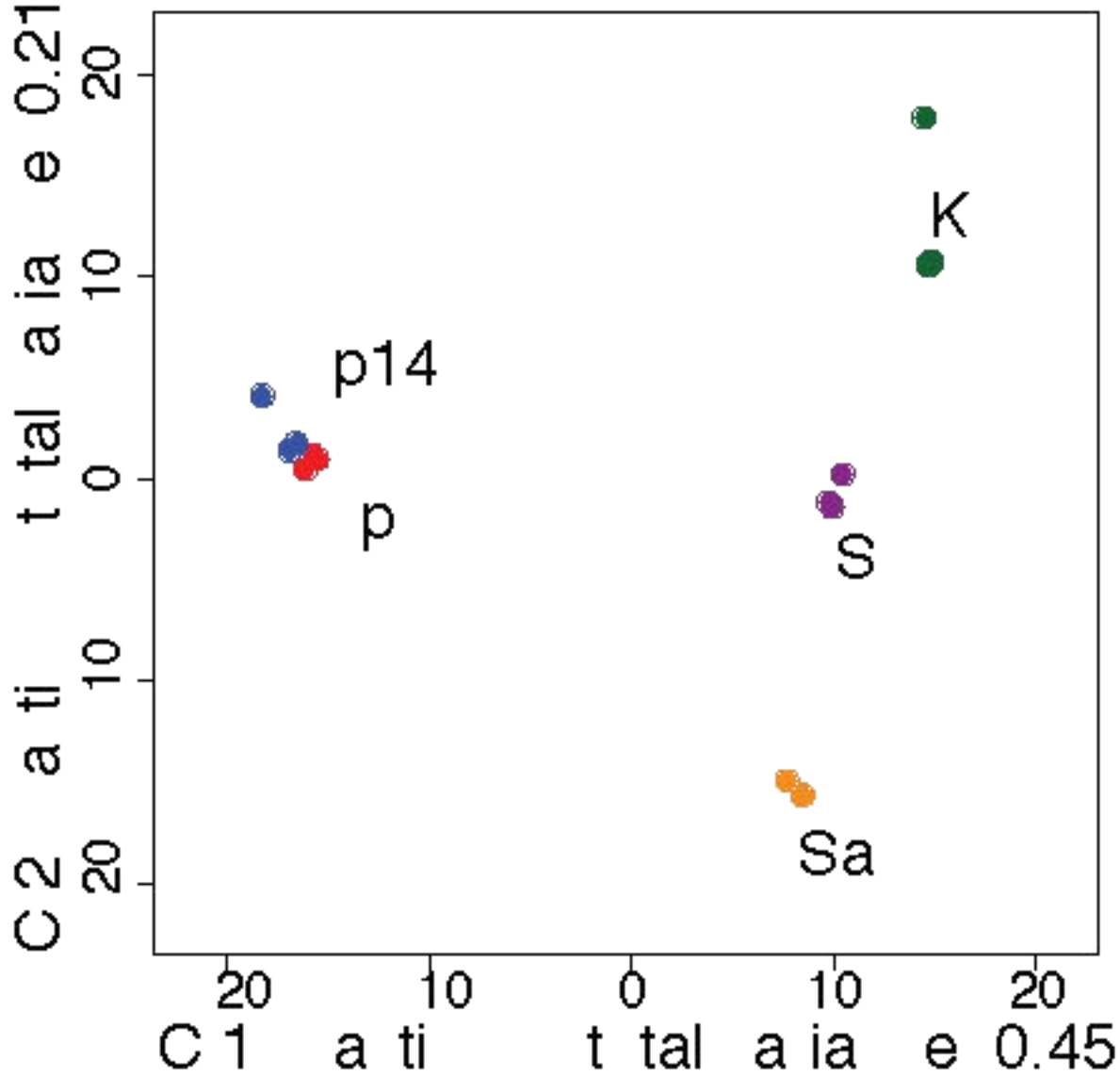

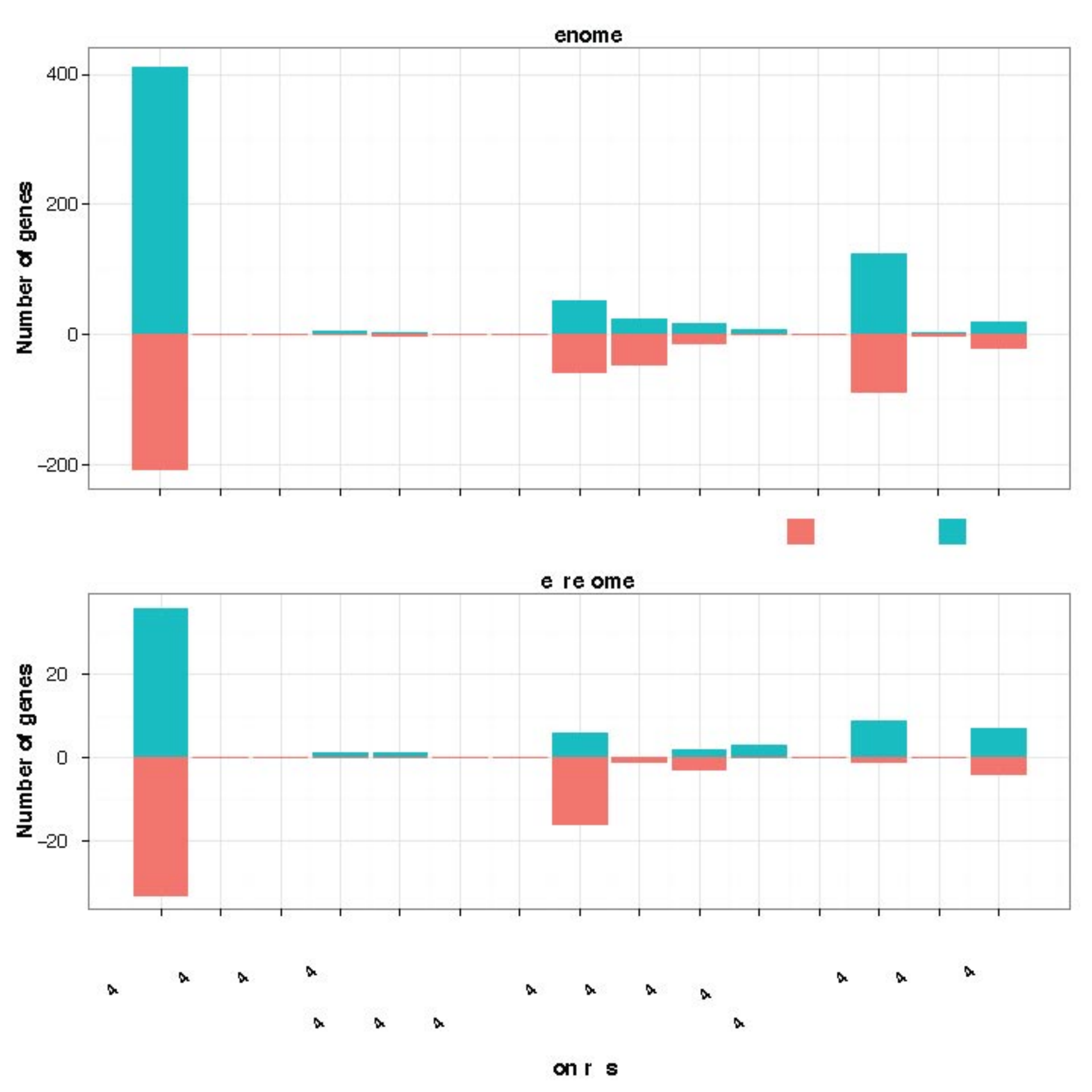
enome
400
200
0
−200
Number of genes
e re ome
20
0
−20
Number of genes
on r s

A

	Gp8	Gp14	K	S	Sa
Antigenic thaumatin–like protein : ARB_01183	6131.2	7203.45	30.04	34.6	257.26
Subtilisin–like protease SUB6 (peptidase S8 family) : ARB_05307	5036.99	2631.96	1.21	1.7	2.79
Uncharacterized protein conserved in filamentous fungi : ARBNEW_231	4218.62	1752.17	0.34	0.1	1375.82
Uncharacterized protein : ARB_03496	4021.16	3952.23	11.68	9.2	17.83
GPI–anchored CFEM domain protein : ARB_02741	3503.48	3821.21	14805.46	8079.51	2149.45
Uncharacterized protein : ARB_05215_05217	3074.2	3499.98	41.92	107.17	215.76
Uncharacterized protein : ARB_02803	3064.4	3092.76	7272.66	6071.91	10321.25
Glycoside hydrolase : ARB_07954	2746.09	4707.54	163.59	866.05	2986.3
GPI–anchored cell wall protein : ARB_01627	2663.98	2756.38	2548.84	1539.09	2111.72
GPI–anchored cell wall protein : ARB_02697	2413.1	3204.93	1052.9	1075.17	1072.41
Ribosomal protein–like : ARB_06463	2092.63	1674.07	827.51	2732.89	3796.79
GPI anchored serine–threonine rich protein : ARB_07696	1628.54	1424.67	3462.73	2765.99	7210.23
1,3–beta–glucanosyltransferase (glycosyl hydrolase 72 family) : ARB_07487	1464.52	1220.67	612.62	529.91	439.93
GPI–anchored CFEM domain protein : ARB_01545	1229.73	1192.05	41.93	331.29	352.46
Neutral protease 2 homolog (peptidase M35 family) : ARB_04336	1156.36	1120.08	12.73	13.09	9.48
1,3–beta–glucanosyltransferase (glycosyl hydrolase 72 family) : ARB_05770	947.52	1298.82	461.92	368.72	411.9
Aspartic–type endopeptidase PEP2 (peptidase A1 family) : ARB_02919	843.45	970.31	691.09	1136.3	549.54
Secreted lipase (type–B carboxylesterase family) : ARB_02369	828.2	291.04	1727.24	561.67	10.69
Subtilisin–like protease SUB10 (peptidase S8 family) : ARB_06467	791.13	789.18	11.62	13.26	12.92
PGA52–like protein (Asp f 4 homolog) : ARB_06390	759.55	749.58	2380.81	1307.5	2003.33
Sialidase : ARB_02206	692.21	1026.03	10.2	5.39	5.24
Extracellular matrix protein : ARB_06538	669.18	911.13	193.05	281.04	699.93
Subtilisin–like protease SUB8 (peptidase S8 family) : ARB_00777	642.2	682.55	188.06	669.86	437.99
Putative stress–responsive protein : ARB_05496	640.41	945.37	16.64	111.83	47.77
NAD–dependent malate dehydrogenase : ARB_00653	615.04	591.45	499.85	820.57	1216.75

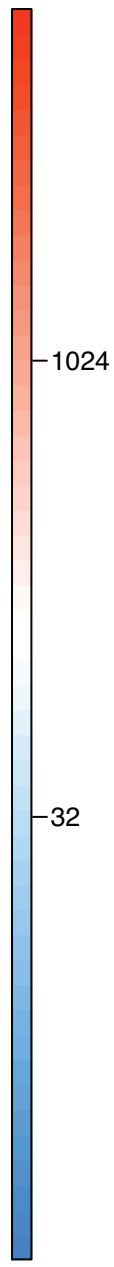

B

	K	Gp8	Gp14	S	Sa
Extracellular serine–threonine rich protein : ARB_04464	18998.65	257.33	202.32	8714.47	4491.1
GPI–anchored CFEM domain–containing protein : ARB_02741	14805.46	3503.48	3821.21	8079.51	2149.45
Subtilisin–like protease SUB3 (peptidase S8 family) : ARB_00701	14610.88	3.14	1.06	480.52	6.78
GPI–anchored cupredoxin : ARB_05732–1	10424.52	1.49	0	5772.18	7327.84
Subtilisin–like protease SUB4 (peptidase S8 family) : ARB_01032	8947.14	13.79	2.88	2202.73	49.24
Uncharacterized protein : ARB_02803	7272.66	3064.4	3092.76	6071.91	10321.25
Uncharacterized protein also found in T. rubrum : ARBNEW_164	6855.24	31.26	21.24	2399.47	901.77
Uncharacterized protein : ARB_06477	4857.97	317.32	208.33	1119.65	894.74
Extracellular proline–rich protein : ARB_00287	4151.91	19.38	16.72	2129.67	634.51
GPI anchored serine–threonine rich protein : ARB_07696	3462.73	1628.54	1424.67	2765.99	7210.23
Cell wall serine–threonine–rich galactomannoprotein : ARB_04561	3214.38	93.86	31.1	1873.43	2727.56
Leucine aminopeptidase 1 LAP1 (peptidase M28 family) : ARB_03568	3064.29	20.64	35.07	582.67	5.81
Probable extracellular glycosidase : ARB_05253	2954.99	241.44	261.81	1050.91	1522.99
GPI–anchored cell wall protein : ARB_01627	2548.84	2663.98	2756.38	1539.09	2111.72
PGA52–like protein (Asp f 4 homolog) : ARB_06390	2380.81	759.55	749.58	1307.5	2003.33
Uncharacterized protein : ARB_00449	2360.49	112.57	70.9	1119.05	1029.48
Uncharacterized protein : ARB_06937	2279.82	15.62	38.19	1305.48	654.83
Metallocarboxypeptidase MCPA (peptidase M14 family) : ARB_07026_07027	2133.1	44.96	35.41	282.48	5.12
Aspartic–type endopeptidase OPSB (peptidase A1 family) : ARB_04170	2112.63	58.04	50.79	579.23	888.52
Exo–beta–1,3–glucanase (glycosyl hydrolase 5 family) : ARB_04467	1818.36	380.53	286.59	427.51	86.85
Extracellular metalloprotease (peptidase M43B family) : ARB_05317	1796.25	80.29	59.69	470.8	6.88
Leucine aminopeptidase 2 LAP2 (peptidase M28 family) : ARB_00494	1792.08	37.5	32.86	2387.84	36.43
Secreted lipase (type–B carboxylesterase family) : ARB_02369	1727.24	828.2	291.04	561.67	10.69
GPI anchored serine–rich protein : ARB_05667	1394.28	575.78	479.78	1935.09	3152.56
Extracellular metalloprotease/fungalysin MEP3 (peptidase M36 family) : ARB_05085	1370.48	1.75	1.21	34.71	6.55